

Smooth transition between SMM and SCM-type slow relaxing dynamics for a 1-D assemblage of {Dy(Nitronyl Nitroxide)₂} units

Ruina Liu, Licun Li, Xiaoling Wang, Peipei Yang, Chao Wang, Daizheng Liao Jean-Pascal Sutter**

Contents

Synthesis of 2-[4-(1-imidazole)phenyl]-4,4,5,5-tetramethylimidazoline-1-oxyl-3-oxide (NITPhIm)

Synthesis of [$\{\text{Gd}(\text{hfac})_3\}_2(\text{NITPhIm})_2$] **1** (same procedure applies for [$\{\text{Dy}(\text{hfac})_3\}_2(\text{NITPhIm})_2$] **2**)

Crystal data for **1** and **2**.

Theoretical expression of the susceptibility used for complex **1**:

Figure S1. The ORTEP drawing (30 % level) of the radical ligand with atom-labelling.

Figure S2. Plot of $\chi_M T$ and χ_M^{-1} vs. T for the radical ligand. The magnetic susceptibility data obey the Curie-Weiss law with a value of the Weiss constant $\theta = -4.92$ K and $C = 0.32$ cm³ K mol⁻¹.

Figure S3. ORTEP plot (50 % level) for [$\text{Gd}(\text{hfac})_3(\text{NITPhIm})_2$] **1**. Hydrogen and fluorine atoms are omitted for clarity.

Figure S4. Molecular Structure of [$\text{Dy}(\text{hfac})_3(\text{NITPhIm})_2$] **2**. Hydrogen and fluorine atoms are omitted for clarity.

Figure S5. Crystal packing of the chains in **2**. Hydrogen and fluorine atoms are omitted for clarity.

Figure S6. The M versus H plot for **1** at 2.0K.

Figure S7. Energy levels $E(S, S')$ of the Rad-Gd-Rad unit in **1**.

Figure S8. Real χ'_M and imaginary χ''_M ac magnetic susceptibilities as a function of temperature for **1** at an ac field of 3 Oe and zero dc field.

Figure S9. The M versus H plot for **2** at 2.0K.

Figure S10. Temperature dependence of the ac susceptibility at different frequencies for **2** under zero dc field.

Figure S11. Argand plot (χ_M'' versus χ_M') at different temperatures. Simulations (full lines) were performed using the conventional generalized Debye model taking into account the width of the τ distribution using α parameters.

Synthesis of 2-[4-(1-imidazole)phenyl]-4,4,5,5-tetramethylimidazoline-1-oxyl-3-oxide (NITPhIm)

2,3-Bis(hydroxylamino)-2,3-dimethylbutane (0.43g, 2.9mmol) and 4-(1*H*-Imidazol-1-yl)benzaldehyde (0.5g, 2.9 mmol) were dissolved in 25 mL methanol. The solution was stirred overnight at room temperature and resulted in white precipitates. 1,3-dihydroxy-2-[4-(1-Imidazole)phenyl]-4,4,5,5-tetramethylimidazoline was obtained as white powder. The white powder was suspended in 100 mL CH₂Cl₂, then added 10g PbO₂. The resulting mixture was stirred for 5 h and then filtered, and the dark blue filtrate was collected. The solvent was removed to obtain deep blue solid. Yield: 65%. m.p.:198-200 °C. Anal. Calc. for C₁₆H₁₉N₄O₂: C, 64.21; N, 18.73; H, 6.69. Found: C, 63.91; N, 18.60; H, 6.40. Single crystals suitable for a X-ray diffraction study were grown by slow evaporation of a solution of the radical in hexane-diethyl(1:1) at room temperature. FT-IR (KBr, cm⁻¹): 3131(w), 2852(m), 1744(s), 1606(s), 1271(s), 842(m), 619(m).

Synthesis of [{Gd(hfac)₃}₂(NITPhIm)₂] **1 (same procedure applies for [{Dy(hfac)₃}₂(NITPhIm)₂] **2**)**

A solution of Gd(hfac)₃·2H₂O or Dy(hfac)₃·2H₂O (0.04 mmol) in 30 mL dry boiling heptane was heated to reflux for 2 h. Then the solution was cooled to 80 °C, and a dry CH₂Cl₂ solution of NITPhIm (0.04 mmol) was added. The resulting mixture was stirred for 2 h at this temperature, then cooled to room temperature and filtered. After 2 days, deep blue crystals were obtained. Yield: 70% for **1** and 63% for **2**. Anal. Calc. for C₆₂H₄₄F₃₆N₈O₁₆Gd₂ (**1**): C, 34.54; N, 5.20; H, 2.06. Found: C, 34.46; N, 5.25; H, 2.13. Anal. Calc. for C₆₂H₄₄F₃₆N₈O₁₆Dy₂ (**2**): C, 34.38; N, 5.17; H, 2.05. Found: C, 34.42; N,5.27; H, 2.12

Crystal data

Crystal data for **1**: C₆₂H₄₄F₃₆Gd₂N₈O₁₆, $M_r = 2155.55$, monoclinic, space group $P2_1/n$, $a = 20.212(4)$ Å, $b = 18.362(4)$ Å, $c = 22.304(5)$ Å, $\beta = 103.18(3)^\circ$, $V = 8060(3)$ Å³, $Z = 4$, $\rho_{\text{calcd}} = 1.776\text{g/cm}^3$, $\mu = 1.780\text{mm}^{-1}$, $T = 113(2)\text{K}$, GOF = 1.096, 46071 reflections collected, 14196 unique (R(int) = 0.0575), R1 = 0.0450, wR2 = 0.0946 [$I > 2\sigma(I)$].

Crystal data for **2**: C₆₂H₄₄F₃₆N₈O₁₆Dy₂, $M_r = 2166.05$, monoclinic, space group $P2_1/n$, $a = 20.154(4)$ Å, $b = 18.309(4)$ Å, $c = 22.199(4)$ Å, $\beta = 102.97(3)^\circ$, $V = 7983(3)$ Å³, $Z = 4$, $\rho_{\text{calcd}} = 1.802\text{g/cm}^3$, $\mu = 2.008\text{mm}^{-1}$, $T = 113(2)\text{K}$, GOF = 1.108, 45011 reflections collected, 14055 unique (R(int) = 0.1986), R1 = 0.0885, wR2 = 0.2026 [$I > 2\sigma(I)$].

Theoretical expression of the susceptibility used for complex 1:

$$\chi' = \frac{Ng^2\beta^2}{6kT} \frac{252\exp(9J_1/2kT - J_2/kT) + 495\exp(8J_1/kT) + 252\exp(7J_1/2kT) + 105}{8\exp(9J_1/2kT - J_2/kT) + 10\exp(8J_1/kT) + 8\exp(7J_1/kT) + 6} + \frac{Ng^2\beta^2}{3kT} S_{Ga}(S_{Ga} + 1)$$

$$\chi_M = \chi' / [1 - (zJ'\chi' / Ng^2\beta^2)]$$

Figure S1. The ORTEP drawing (30% level) of the radical ligand with atom-labelling.

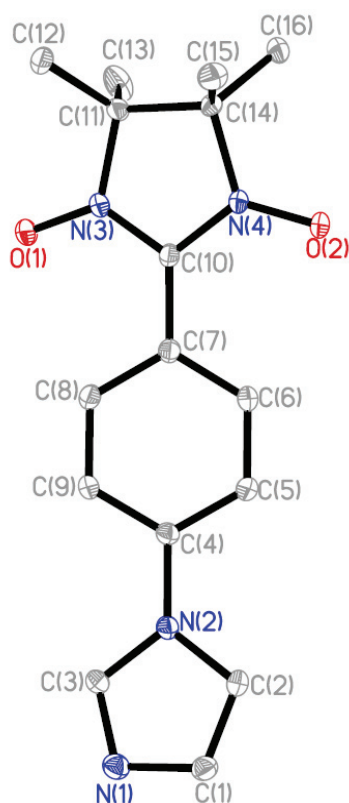


Figure S2. Plot of $\chi_M T$ and χ_M^{-1} vs. T for the radical ligand. The magnetic susceptibility data obey the Curie-Weiss law with a value of the Weiss constant $\theta = -4.92$ K and $C = 0.32$ cm³ K mol⁻¹.

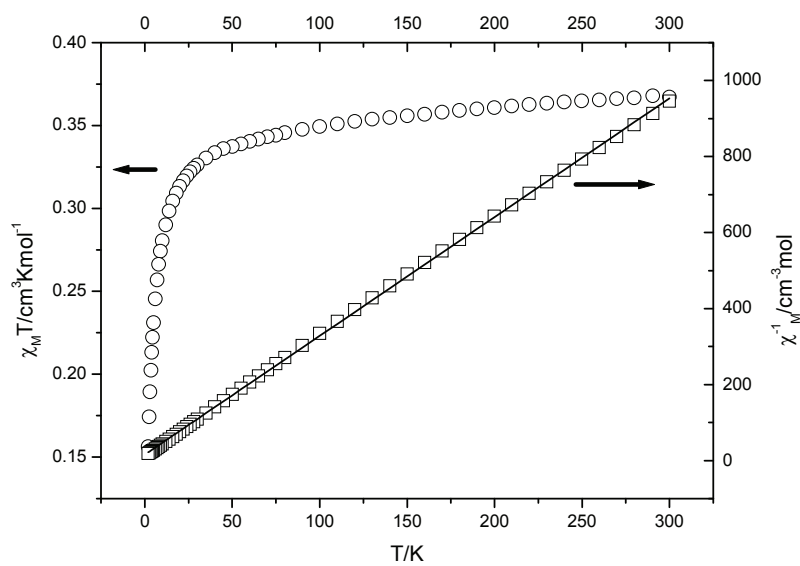


Figure S3. ORTEP plot (50% level) for $[\text{Gd}(\text{hfac})_3(\text{NITPhIm})_2]$ **1**. Hydrogen and fluorine atoms are omitted for clarity.

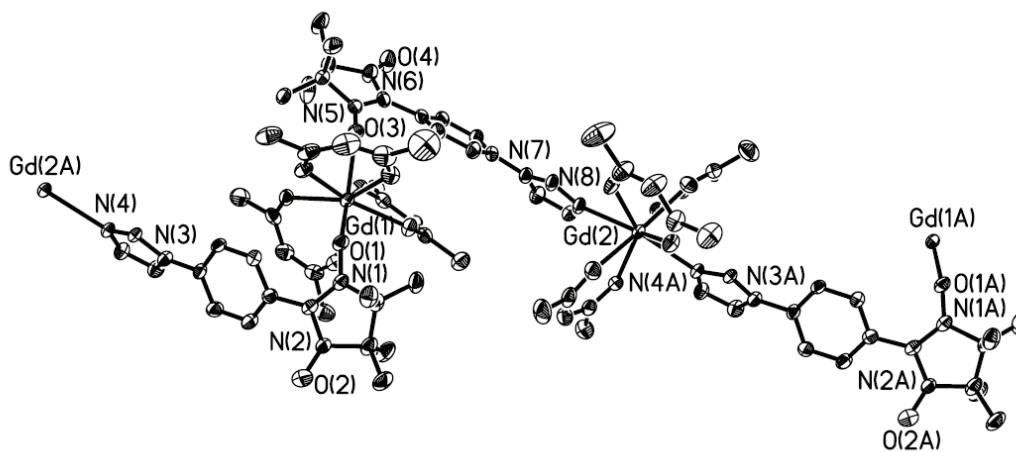


Figure S4. Molecular Structure of $[\text{Dy}(\text{hfac})_3(\text{NITPhIm})_2]_2$ **2**. Hydrogen and fluorine atoms are omitted for clarity.

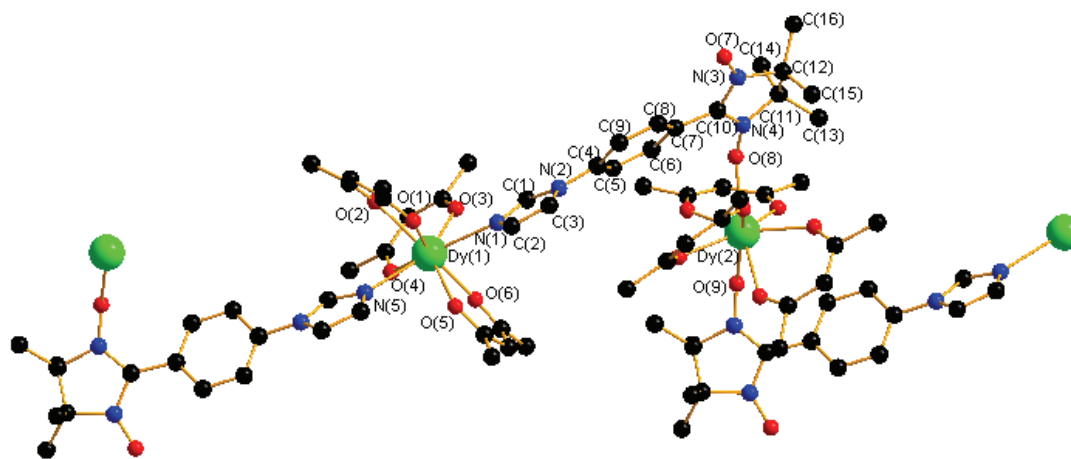


Figure S5. Crystal packing of the chains in **2**. Hydrogen and fluorine atoms are omitted for clarity.

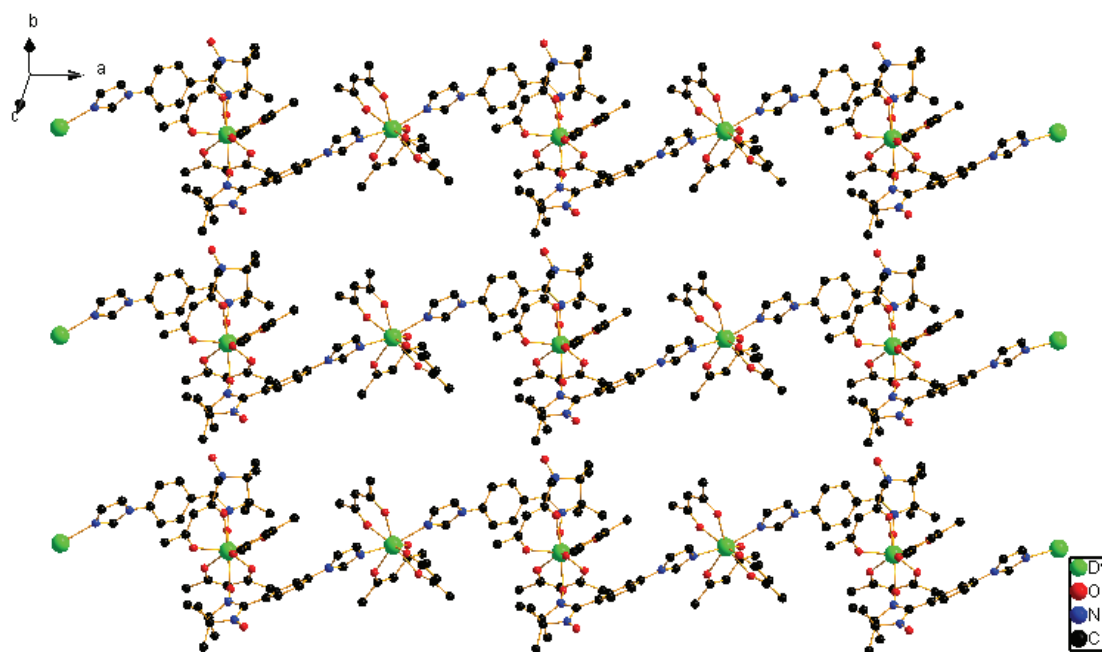


Figure S6. The M versus H plot for **1** at 2.0K.

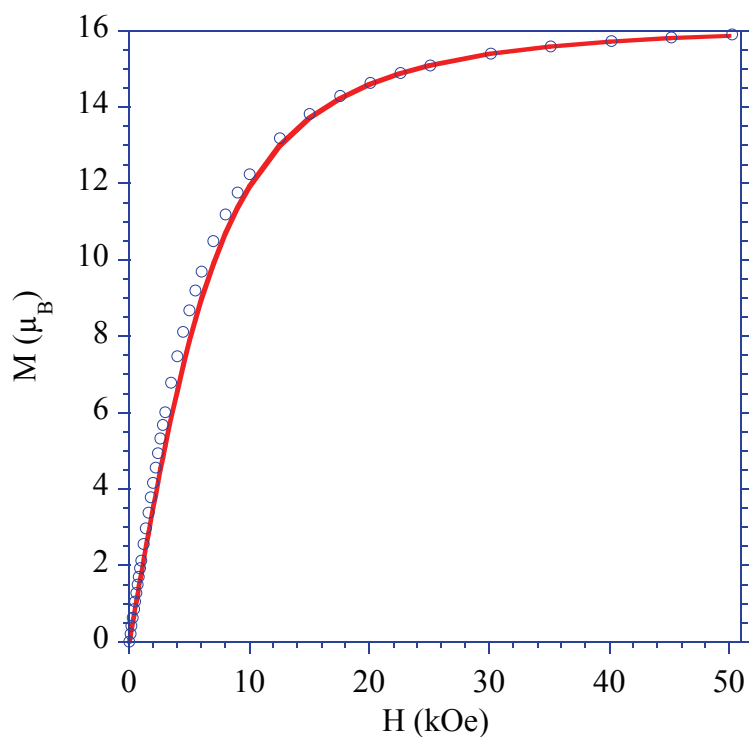


Figure S7. Energy levels $E(S, S')$ of the Rad-Gd-Rad unit in **1**.

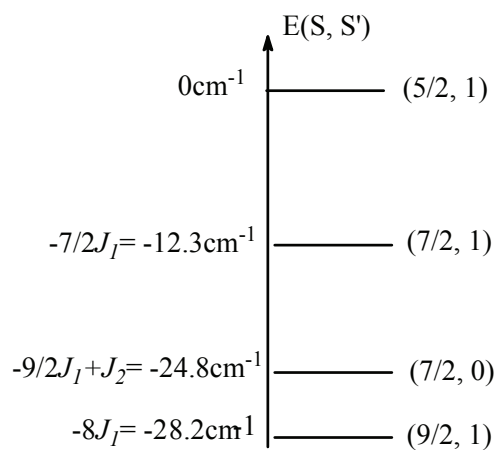


Figure S8. Real χ'_M and imaginary χ''_M ac magnetic susceptibilities as a function of temperature for **1** at an ac field of 3 Oe and zero dc field.

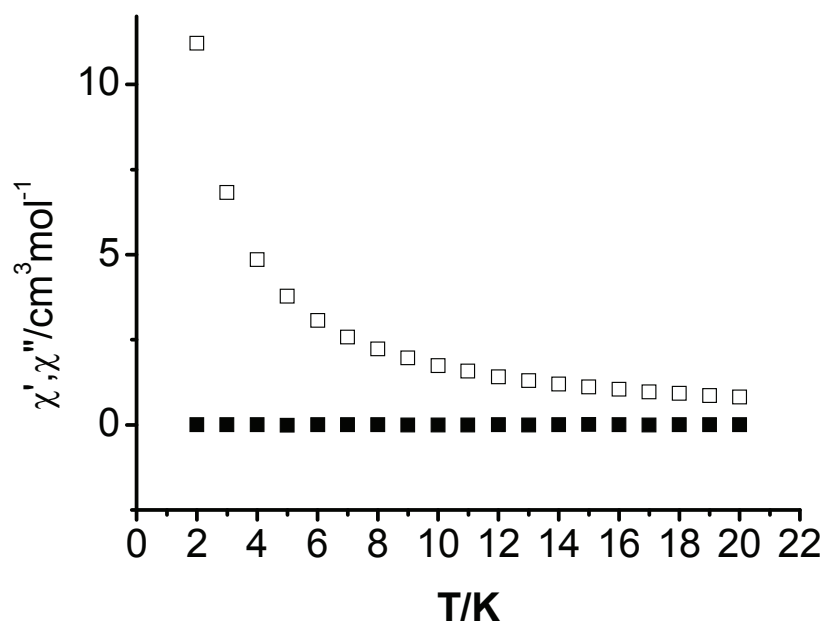


Figure S9. The M versus H plot for **2** at 2.0K.

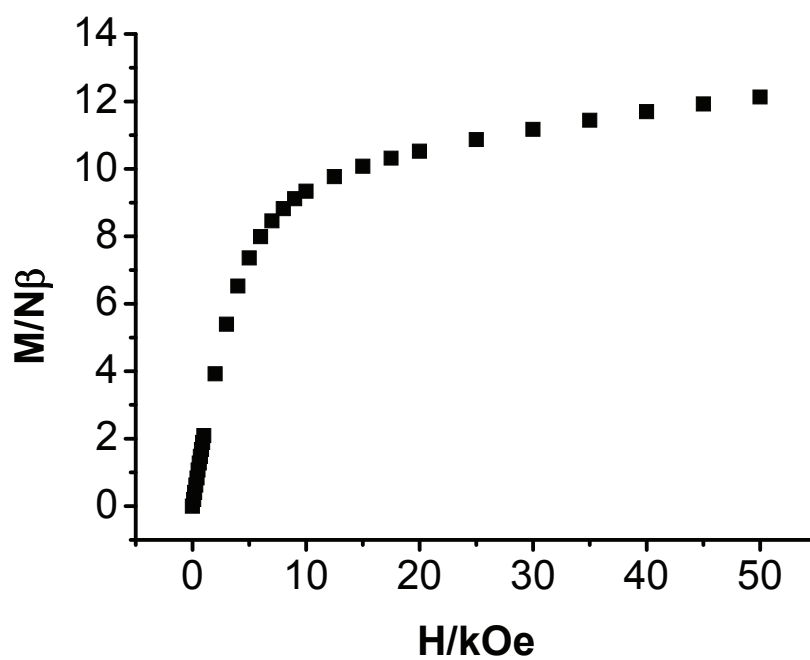


Figure S10. Temperature dependence of the ac susceptibility at different frequencies for **2** under zero dc field.

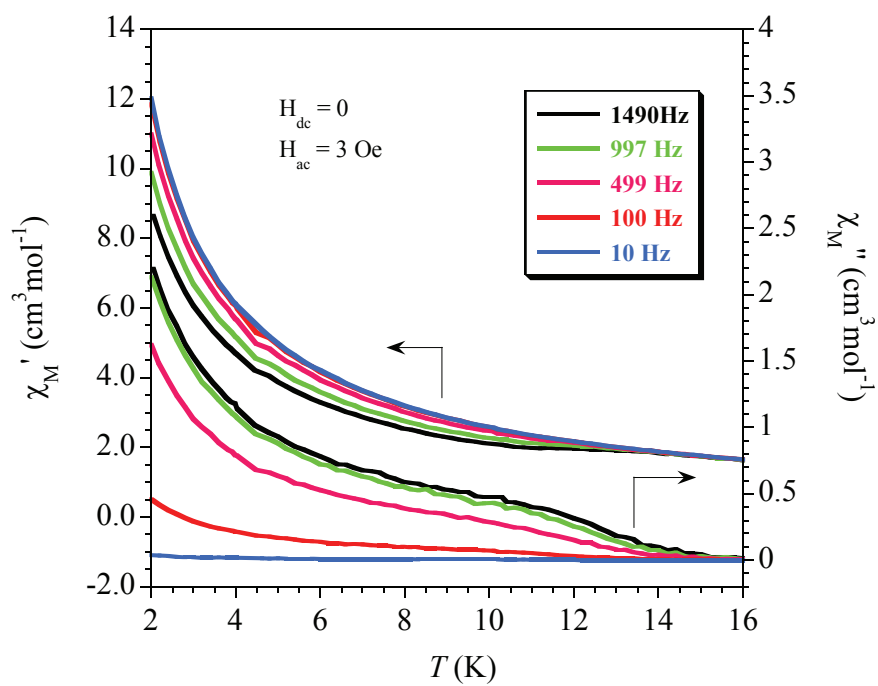
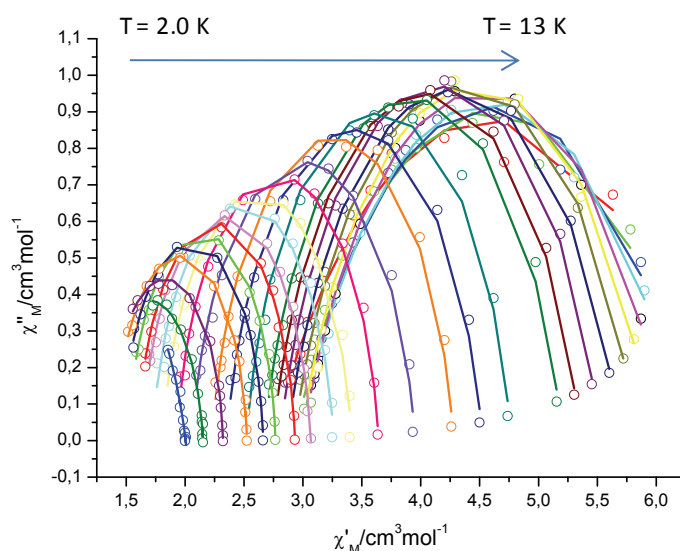


Figure S11. Argand plot (χ_M'' versus χ_M') at different temperatures. Simulations (full lines) were performed using the conventional generalized Debye model taking into account the width of the τ distribution using α parameters.¹



Fitting parameters:

T/K	χ_0	χ_∞	α
2.0	6.42	2.73	0.43
2.2	6.29	2.92	0.37
2.4	6.26	2.95	0.36
2.6	6.20	2.98	0.33
2.8	6.07	3.00	0.29
3.0	5.96	2.98	0.27
3.2	5.84	2.92	0.25
3.4	5.70	2.86	0.24
3.6	5.52	2.80	0.21
3.8	5.36	2.74	0.20
4.0	5.21	2.67	0.19
4.4	4.77	2.52	0.14
5.0	4.52	2.35	0.15

5.4	4.28	2.23	0.14
6.0	3.95	2.06	0.14
6.6	3.64	1.93	0.11
7.1	3.42	1.81	0.11
7.5	3.26	1.72	0.11
8.1	3.07	1.63	0.10
8.5	2.93	1.60	0.07
9.1	2.77	1.52	0.06
9.5	2.66	1.47	0.06
10	2.53	1.40	0.065
11	2.32	1.34	0.06
12	2.15	1.25	0.10
13	2.00	0.62	0.22

References

¹ D. Gatteschi, R. Sessoli, J. Villain in *Molecular Nanomagnets*, Oxford University Press **2006**. D. Gatteschi, R. Sessoli *Angew. Chem. Int. Ed.* **2003**, *42*, 269-297. R. Sessoli, A.K. Powell *Coord. Chem. Rev.* **2009**, *253*, 2328-2341.